

1 Shape optimization for improved
2 understanding of magmatic plumbing
3 systems

4 **Théo Perrot, Freysteinn Sigmundsson**
5 June 2024

6 **Abstract**

7 Inverse problems in volcanic geodesy are crucial for identifying the location
8 and shape of magmatic bodies based on ground deformation data. Tra-
9 ditional approaches often rely on models with predefined shapes, which can
10 limit their accuracy. To address this, we present a shape optimisation method
11 using a level-set approach that flexibly determines the optimal shape of a
12 magma chamber without prior shape assumptions. By minimising the dis-
13 crepancy between observed and modelled surface displacements, our adapted
14 algorithm becomes suitable for solving inverse volcano deformation problems.
15 We explore the capabilities of this approach with synthetic data and apply it
16 to InSAR observations of the Svartsengi volcanic system in Iceland, demon-
17 strating its potential to improve volcanic hazard assessment after maturation
18 through future work.

19 **1 Introduction**

20 **1.1 Challenge**

21 In volcano geodesy, inverse problems are central to estimating the position
22 of magmatic bodies using ground motion as a proxy. Displacement is ob-
23 served by geodetic measurements such as Global Navigation Satellite System
24 (GNSS) point positioning, leveling campaigns, or Synthetic Aperture Radar
25 (InSAR) interferometry within a volcanic field, and the subsurface processes
26 causing the movement are inferred from these observations (Dzurisin 2007).
27 Magmatic sources are modeled as pressurized cavities that deform the sur-
28 rounding host rocks and cause the surface to move. Various inversion meth-
29 ods based on parametric analytical or numerical models aim at finding the
30 optimal values for the vector of d free parameters $\vec{m} \in \mathbb{R}^d$ of the model. Then
31 an error function $J(\vec{m})$ is representative of the misfit between the observed
32 displacements and the prediction of the model. \vec{m}_{opt} can then be found using
33 various inversion techniques that minimize J : global optimization based on
34 analytic (Cervelli et al. 2001) or numerical models (Hickey and Gottsmann
35 2014, Charco and Galán del Sastre 2014), Bayesian inference (Bagnardi and
36 Hooper 2018, Trasatti 2022), or genetic algorithms (Velez et al. 2011) on
37 analytic models. The choice of the method is constrained by the reasonable
38 number of evaluations of $J(\vec{m})$: numerical models handle a complex descrip-
39 tion of the system, but are computationally expensive compared to analytic
40 models, which on the other hand may lead to an oversimplification (Taylor,
41 Johnson, and Herd 2021).

42 However, each of these finite-dimensional optimization methods is limited
43 by the intrinsic assumption of a definite parametric shape for the source. In
44 fact, analytic expressions can be derived for only a few regular shapes such as
45 point source (Mogi 1958), finite sphere source (McTigue 1987), or ellipsoidal
46 source (Yang, Davis, and Dieterich 1988), and any numerically generated
47 shape must be parameterized to be inverted. Even in the case where complex
48 shapes are chosen, they would require additional describing parameters, and
49 ultimately any of the above methods may face the curse of dimensionality.
50 The goal of this paper is not to give a definitive answer to these limitations,
51 but rather to lay the first stone for a new approach that overcomes these
52 difficulties.

53 **1.2 Shape optimization**

54 Shape (and topology) optimization aims to find the shape that minimizes a
55 given function defined on a given system, without the need for prior assump-

tions about shape and topology. It is actively developed by part of the applied mathematics community and is widely used in engineering to find optimal designs for systems: In structural mechanics, to maximize the stiffness of a solid structure such as a cantilever beam (Bendsøe and Ole Sigmund 2004), in fluid-structure interaction on heat exchangers or flying obstacles (F. Feppon et al. 2020), and even as a way to explore new architecture for buildings (Beghini et al. 2014). Most finite element simulation and design software now implements an embedded shape optimization module (Frei 2015, Slavov and Konsulova-Bakalova 2019, Le Quilliec 2014). However, its use has not yet been reported in the context of inverse problems in volcano geodesy, where it can overcome the shape hypothesis problem as long as an internal pressure value is assumed.

Many paradigms coexist in shape optimization as reviewed by Ole Sigmund and Maute 2013, one of the most popular being SIMP optimization, where a density value is optimized for each element of the mesh with values between 0 (void) and 1 (material) before being black and white filtered to output a design (O. Sigmund 2001, Bendsøe and Ole Sigmund 2004), with several open source implementations (Andreassen et al. 2011, Hunter et al. 2017). We chose level-set shape optimization instead because it has the advantage of providing an explicit representation of the boundary at each step of the optimization, which is crucial for us as explained later (section 2). For this, we relied on the work of Dapogny and Florian Feppon 2023, who thoroughly described and vulgarized the method, as well as providing a freely available open source implementation of the method, `sotuto`(Dapogny and Florian Feppon 2024), which we modified and extended to adapt it to inverse geodetic problems.

2 Method

Here we briefly present the key ingredients of level set shape optimization along with their implications for our problem. The full mathematical background on which it relies is not detailed, but see this chapter by Allaire, Dapogny, and Jouve 2021 for a comprehensive step-by-step description supported by proofs and theorems. It is also worth noting that many aspects of secondary importance to the method are not mentioned for the sake of brevity. For the unfamiliar reader interested in understanding the method, the lecture (especially part III) given by Dapogny and Bonnetier 2024 at the Université Grenoble Alpes is also recommended.

92 **2.1 Model**

93 Let Ω be a bounded domain of \mathbb{R}^3 whose shape we want to optimize by
94 modifying parts of its boundary $\partial\Omega$. As for classical analytical models of
95 volcanic deformation induced by magmatic activity, Ω is a domain represent-
96 ing a portion of the shallow Earth crust, including the volcano, assumed
97 to be homogeneous, isotropic, and elastic. The governing equations are
98 $-\operatorname{div}(Ae(u)) = 0$ in Ω , where $e(u)$ is the strain tensor of the displacement
99 field u and A is the constitutive law tensor, $Ae = 2\mu e + \lambda \operatorname{tr}(e)Id$ for linear
100 elasticity. Boundaries under different conditions, see Fig. 1 for all notations.

101 The part of $\partial\Omega$ to be optimized is Γ_s , the boundary magma chamber,
102 which is modeled as an empty, uniformly pressurized cavity. Therefore, a
103 value for the internal pressure ΔP must be assumed (see Discussion for devel-
104 opment). In the following text we talk about optimizing $\partial\Omega$, but in practice
105 only $\Gamma_s \subset \partial\Omega$ is of interest and will be modified, any other boundary will be
106 fixed during the iterations.

107 We want to find $\partial\Omega$ such that the displacement of the model $u(\Omega)$ is as
108 close as possible to the observed displacement u_o on the surface Γ_u . Thus,
109 the unconstrained shape optimization problem we want to solve is the mini-
110 mization of a squared RMS discrepancy

$$\min_{\Omega} J(\Omega) = \int_{\Gamma_u} (u(\Omega) - u_o)^2 dS \quad (1)$$

111 **2.2 Hadamard Boundary Variation**

112 Overall, this method can be considered a classical iterative gradient descent
113 algorithm. J is first initialized at J_0 with an instructed first guess for Ω_0 and
114 then iteratively decreased by moving $\partial\Omega$ of a given step in a given descent
115 direction $\theta : \mathbb{R}^3 \mapsto \mathbb{R}^3 \in W^{1,\inf}$ (the Sobolev space of uniformly bounded
116 functions, Allaire, Dapogny, and Jouve 2021) chosen using the shape deriva-
117 tive $J'(\Omega)(\theta)$.

118 The boundary variation method of Hadamard 1908 introduces the notion
119 of shape differentiation $F'(\Omega)(\theta)$ of a functional F defined on Ω in the di-
120 rection θ . In short, such a derivative is based on the variation of a bounded
121 domain $\Omega \mapsto \Omega_\theta := (Id + \theta)(\Omega)$: the surface $\partial\Omega$ is slightly moved according
122 to a small vector field $\theta(x)$, as shown in Fig. 2. Once such a derivative
123 exists, one can compute a descending direction at the n^{th} step θ_n , such as
124 $J'(\Omega)(\theta_n) \leq 0$, so $J_{n+1} \leq J_n$, to decrease the value of J at each iteration.

125 In our case, after derivation based on the Cea 1986 formal method, we

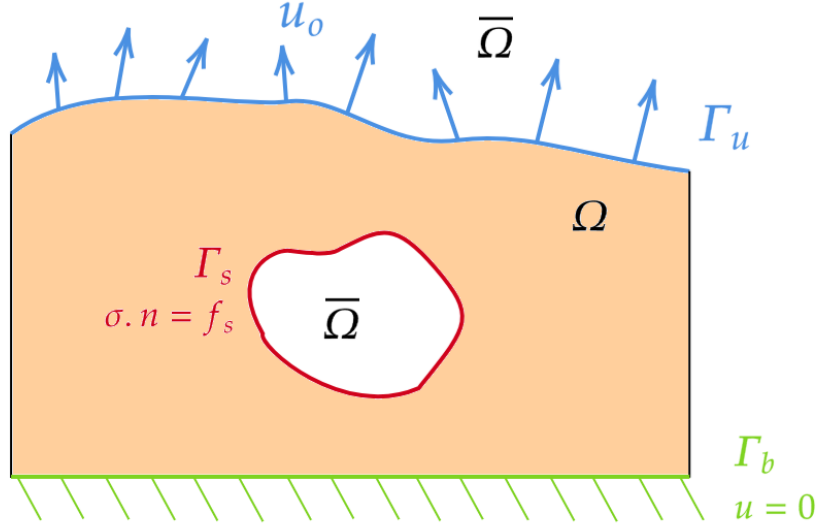


Figure 1: 2D sketch of the problem. The optimized boundary (where the level-set function is zero) is the magma chamber wall Γ_s subjected to a uniform normal load $\sigma(u).n = f_s$ on Γ_s , where $f_s = -\Delta P.n$, where n is the unit normal vector and ΔP is the pressure change between the magma source and the surrounding crust. The bottom surface Γ_b is fixed ($u = 0$). The other boundaries are free. The target displacement field u_o is known on the upper surface Γ_u .

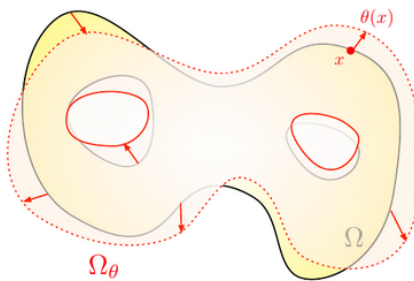


Figure 2: Reproduced from Allaire, Dapogny, and Jouve 2021

¹²⁶ found under the variational form :

$$J'(\Omega)(\theta) = \int_{\Gamma_s} \left(Ae(u) : e(p) + \frac{\partial f_s}{\partial n} p + \frac{\partial p}{\partial n} f_s + \kappa f_s p \right) . \theta . n dS \quad (2)$$

127 where $\kappa = \operatorname{div}(n)$ is the mean curvature at the boundary, and p is the
128 adjoint solution of

$$\forall v \in H^1(\mathbb{R}^3), \int_{\Gamma_u} 2(u_\Omega - u_o)v dS + \int_{\Omega} Ae(v) : e(p) dV = 0 \quad (3)$$

and $p = 0$ on Γ_b

129 From there, we can trivially move Ω in the direction $\theta = -A$ (where
130 A is the integrand term in parentheses) to ensure that $J'(\Omega)(\theta) \leq 0$. This
131 guarantees that $J(\Omega_{n+1}) \leq J(\Omega_n)$: the series $J(\Omega_n)$ converges to a minimum.

132 2.3 Level-set representation

133 A key issue is the representation of the surface to be optimized. The level
134 set method allows to track dramatic changes as well as topology variations
135 (creation of new holes). A certain function $\phi : D \mapsto \mathbb{R}$ is defined over the
136 domain $D \in \mathbb{R}^3$ in such a way that the shape boundary is the level set 0,
137 i.e. reads $\partial\Omega = \phi(x = 0)$. Basically, ϕ can be taken as the signed distance
138 between any point x and $\partial\Omega$, as shown in the example fig. 3. In this way,
139 $\partial\Omega$ is implicitly manipulated when transforming ϕ .

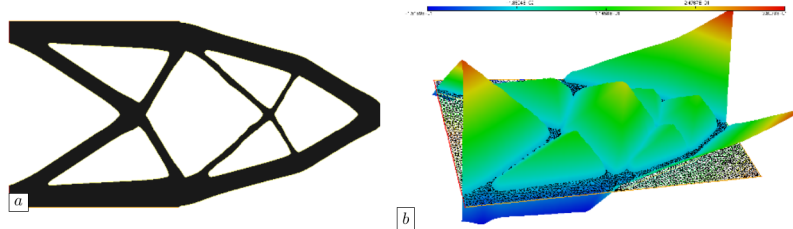


Figure 3: Reproduced from Dapogny and Florian Feppon 2023

140 Ω_n is then deformed by advecting the corresponding ϕ_n with a velocity
141 field $V(x) = \tau_n \theta_n$, where τ_n is the additional step size. The advection equa-
142 tion usually appears in fluid mechanics to describe the evolution of a quantity
143 transported by a given velocity field, but here there is a smooth and flexible
144 way to modify ϕ which ensures smoothness of Ω_{n+1} and change of topology
145 (see Allaire, Dapogny, and Jouve 2021).

146 **2.4 Numerical implementation**

147 **2.5 Numerical implementation**

148 In practice, the D domain is discretized into a mesh T_n on which each variational form is solved at each iteration n . This includes the solution of the elasticity to get u_n , the adjoint state p_n , the computation of the shape gradient J'_n , the descent direction θ_n , the advection of ϕ_n . In **sotuto** it is achieved by calling scripts written in FreeFem++, a finite element software that allows solving any integral form of elliptic PDE (Hecht 2012).

154 Once the new form Ω_{n+1} is computed and discretized thanks to a local remeshing phase, a new evaluation of J^{n+1} is performed. Since τ is arbitrarily fixed and initialized to 1, it can happen that Ω_n is shifted by too large a step and so $J_{n+1} \geq J_n$. To adjust the step size, a line search procedure is implemented and adjusts the step size by decreasing it if the new iteration is the worst to ensure an improvement of J by computing a new Ω_{n+1} being a less deformed version of Ω_n . On the contrary, if Ω_{n+1} is accepted, τ is increased to speed up convergence. A tolerance is set to accept iterations if the increase in J is reasonable.

163 The global optimization loop has no termination criterion. Thus, it is up to the user to stop it when no significant improvement in J can be achieved, or when the shape is not realistic.

166 The loop and the line search are implemented in Python in **sotuto**. Then the FreeFem scripts are called by the Python script core and data is exchanged via temporary files.

169 The above aspects are implemented in **sotuto**. However, we extended its functionality to handle our geophysical problem, in a fork we called **magmaOpt**. This included: scripts to create the domain and initial source with GMSH Geuzaine, Remacle, and Dular 2009 ,adapting FreeFem scripts to different error functions, allowing optimization of the loaded boundary Γ_s and so on.

174 **3 Validation with synthetic data**

175 To test the method, the idea is to do a kind of cross-validation. On the one hand, the observation data is a synthetic 3D displacement field for which we know the source parameter. On the other hand, we initialize the algorithm with a first guess for the source shape and location. We expect the algorithm to iteratively modify the shape of the source and converge to the correct shape and location. In fact, the 3D location of the source (e.g., its center of gravity for a random shape) is not directly optimized as a vector of discrete parameters, but is modified by the simple fact that the boundary is free to

183 move in any direction, and thus can take on a kind of "average rigid body
184 motion" as it gradually moves the center in a given direction.

185 In practice, the synthetic observed surface displacement field is derived
186 from the Mc Tigue solution, an analytical approximation of the displacement
187 caused by a uniformly pressurized spherical cavity (the magma domain) em-
188 bedded in an isotropic, homogeneous, and planar elastic medium (the host
189 crust) McTigue 1987 with elastic constants $\text{tp } E = 10\text{GPa}$ and $\mu = 0.25$.

190 Usually, the quantities to be determined with parametric inversion based
191 on a McTigue model are the location and the radius. The pressure change
192 can also be left as a free parameter, but is interchangeable with the radius,
193 so one must be fixed to determine the other, see (Greiner 2021) for more
194 details. For the synthetic source, we fixed these free parameters to $z = -5\text{km}$,
195 $\Delta P = 10\text{MPa}$, $R = 1.5\text{km}$, which are typical values for inverted magmatic
196 domains.

197 On the other hand, to test the robustness of the method, we tried different
198 initial Ω_0 shapes. The tests included: same center but different shape, dif-
199 ferent center but same shape, and different shape and center, as summarized
200 in the table ??.

201 `magmaOpt` is then allowed to run freely, without any termination condition,
202 to see whether or not it succeeds in converging from the ellipsoid to the
203 McTigue sphere we used to generate the synthetic displacement.

204 Since there is no termination condition here, we take the shape corre-
205 sponding to the smallest value of J found as the best result (although it can
206 be discussed, see the conclusion). To evaluate the quality of the result, we use
207 two different metrics. On the one hand, the distance between the centroids
208 of the final source and the synthetic sphere is an indicator of the distance
209 between the two corps and assesses whether the final shape taken as a rigid
210 body is overall correctly located. On the other hand, after aligning the final
211 source surface on the sphere using an iterative point cloud (ICP) algorithm,
212 we use the chamfer distance to asses the difference in terms of shape.

213 4 Real test case : Svartsengi 2022 inflation

214 We now apply the method to infer the shape of a magma domain in a recent
215 period of volcanic unrest and eruption in SW Iceland by evaluating the shape
216 of a magma body responsible for the ground inflation observed from 21 April
217 to 14 June 2022 at Svartsengi on the Reykjanes peninsula. This is one of
218 5 inflation episodes that preceded catastrophic dike breaches and eruptions
219 at the Sundhnúkur crater row, which caused the destruction of the city of
220 Grindavík (Sigmundsson et al. 2024).

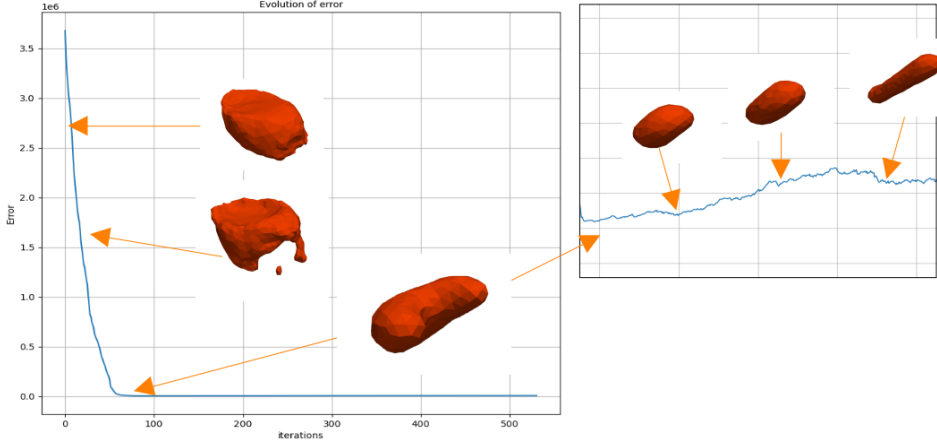


Figure 4: Evolution of error and successive shapes taken by the magma source during an optimization loop. The initial guess is a flat ellipsoid of semi-axes $r_x = 2\text{km}$, $r_y = 3\text{km}$, $r_z = 1\text{km}$ centered on the true spherical source. The minimum is reached at iteration 82.

The observational data used are the line-of-sight (LOS) displacement maps of the area from Cosmo SkyMed available in Parks et al. 2024, the data used in Sigmundsson et al. 2024. After uniform downsampling and mesh reprojection (the data points must be aligned on the mesh nodes), the ascending A32 and descending D132 tracks were both used in the RMS error function we adapted to the LOS geometry.

$$J(\Omega) = \sum_{i \in tck} \alpha_i \int_{\Gamma_u} (L_i(u(x)) - l_o^i(x))^2 dS \quad (4)$$

Where $tck = \{A125, D132\}$. For each track i , α_i is the weight of the track ($\forall i, \alpha_i = 1$ here), $L_i : \mathbb{R}^3 \mapsto \mathbb{R}$ is the function that projects the 3D surface displacement given by the model into the LOS geometry, and l_o^i is the observed LOS displacement.

We then used the framework developed above, only projecting the InSAR data onto the mesh of D and modifying the expression of the error function in `magmaOpt`.

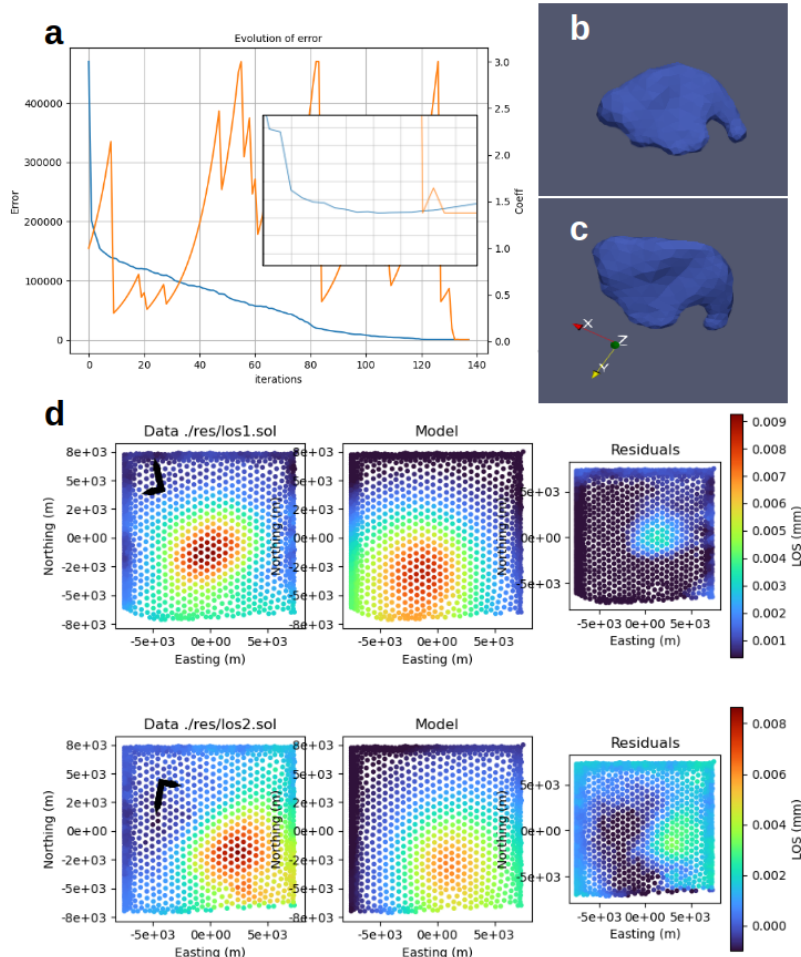


Figure 5: a) Convergence plot with embedded zoom. The blue line is the error and the orange line is the evolution of τ . Minima are reached at iteration 128. b,c) Side and top view of the source Γ_s minimizing J . d) Data, model and residuals of the LOS displacements at iteration 128 for the two InSAR tracks A32 (top) and D132 (bottom). Black arrows are heading and looking directions, coordinates are ISN16 Íslands 2024 shifted to a local origin (2529373E, 179745N).

The results shown in figure 5 are encouraging: after providing an initial guess located at the center of inflation at depth for a sphere of radius RR, the algorithm is able to iteratively change the shape and depth of the magma domain to finally result in a sill-like flattened spheroid whose centroid is located at DD depth. This is consistent with the presumed depth found in the supporting information of Sigmundsson et al. 2024, which performs an

240 analytical model-based inversion. Although the pressure must be fixed, as
241 explained in 1.2, the result can be used to compare the final shape of the
242 magmatic intrusion and give a richer insight into it. Here we see interesting
243 features, such as an increasing thickness on the north side, that can't
244 be traced by any other method. The algorithm produces features that we
245 consider to be artifacts, probably due to mesh refinement problems, such as
246 small holes or horn-shaped features.

247 5 Discussion

248 This work paves the way for a new class of methods that tackle an unknown
249 geometry of the magmatic domains, thus giving the possibility to explore
250 irregular shapes that are more likely to exist compared to any other usually
251 assumed regular shapes. However, even if the first results presented are
252 promising, many questions remain to be answered. First of all, the internal
253 pressure of the chamber must be specified, which is a strong hypothesis.
254 In this context, the precise shape of the source should be determined as a
255 second step. The traditional analytical model-based inversion would be run
256 first, giving a pressure and a first educated guess for the position and shape
257 of Ω_0 . Then a more realistic shape could be sought with a shape optimization
258 taking the output of the inversion as an initial guess.

259 Adding constraints may also be an interesting way to explore. For ex-
260 ample, the volume of the source could be constrained to be within bounds
261 or even to match a certain value. The implemented shape optimization is
262 certainly able to handle constraints as described by [allaire202](#). The physical
263 meaning of the best shape might benefit from a more constrained problem,
264 and the less influencing deeper part of the source might be less random.

265 To better understand the influence of data partitioning and variablitiy,
266 additional tests could be run with synthetic data. We can think of tests
267 such as masking part of the surface displacement field, introducing noise
268 and parasitic signals, reducing the number of data points, as is often the
269 case in reality with areas of volcanic systems lacking data coverage (glacier,
270 river, lava, forest) and subjected to perturbations (atmospheric distortion,
271 weather).

272 It is also important to mention that the behavior of the algorithm is
273 influenced by numerous parameters of varying importance, starting from the
274 discretization length (element size) or the domain extent, to the limits of the
275 step size τ , the regularization length, or the number of iterations allowed by
276 the line search. A systematic study of each of these parameters would be
277 beneficial in assessing the quality of the shape inferred.

278 Exploring a way to quantify the uncertainty of the answer is also crucial.
279 For example, a sensitivity analysis approach could be considered, as well as
280 the inclusion of a probabilistic quantity.

281 6 Conclusion

282 The present study has successfully demonstrated the application of inverse
283 problems and computational methods to infer the shape of a magma domain
284 beneath a volcano using ground inflation data from satellite observations.
285 The shape optimization technique used in this research showed a new way to
286 identify the most likely shape of the magma chamber. It was intended as an
287 opening to new methods rather than a complete solution.

288 We have shown that modifying a shape optimization algorithm to handle
289 geophysical problems is feasible and of interest. Tests on synthetic data
290 showed to some extent the relevance of the approach, although the best
291 sources found exposed the limitations faced by these first attempts of shape
292 optimization for volcano geodesy. The test on real data showed a concrete
293 case of how the method could be used after being more mature.

294 The perspectives are numerous. The numerical nature of the models
295 allows to easily add complexities to the modeling, such as complex mechanical
296 behavior of the crust (plaxticity, viscoelasticity, poroelsaticity), additional
297 loads (tectonic stress, tidal loads, glacier weights), or inhomogeneities. We
298 hope that the open source code `magmaOpt` developed by us will be modified
299 and extended by future work.

300 By addressing these limitations and extending this approach, researchers
301 can further improve the accuracy and reliability of magma domain shape
302 inference. Ultimately, the development of more sophisticated models will
303 enable geophysicists to better monitor volcanic activity, predict eruptions,
304 and provide critical support for hazard mitigation strategies.

305 References

- 306 Allaire, Grégoire, Charles Dapogny, and François Jouve (2021). “Chapter 1
307 - Shape and Topology Optimization”. In: *Geometric Partial Differential
308 Equations - Part II*. Ed. by Andrea Bonito and Ricardo H. Nochetto.
309 Vol. 22. Handbook of Numerical Analysis. Elsevier, pp. 1–132. DOI: 10.
310 1016/bs.hna.2020.10.004. URL: <https://www.sciencedirect.com/science/article/pii/S1570865920300181>.

- 312 Andreassen, Erik et al. (Jan. 2011). "Efficient Topology Optimization in
 313 MATLAB Using 88 Lines of Code". In: *Structural and Multidisciplinary*
 314 *Optimization* 43.1, pp. 1–16. ISSN: 1615-147X, 1615-1488. DOI: 10.1007/
 315 s00158-010-0594-7. URL: <http://link.springer.com/10.1007/s00158-010-0594-7> (visited on 08/22/2024).
- 316
- 317 Bagnardi, Marco and Andrew Hooper (July 2018). "Inversion of Surface De-
 318 formation Data for Rapid Estimates of Source Parameters and Uncer-
 319 tainties: A Bayesian Approach". In: *Geochemistry, Geophysics, Geosys-
 320 tems* 19.7, pp. 2194–2211. ISSN: 1525-2027, 1525-2027. DOI: 10.1029/
 321 2018GC007585. URL: <https://agupubs.onlinelibrary.wiley.com/doi/10.1029/2018GC007585> (visited on 02/29/2024).
- 322
- 323 Beghini, Lauren L. et al. (Feb. 1, 2014). "Connecting Architecture and En-
 324 gineering through Structural Topology Optimization". In: *Engineering*
 325 *Structures* 59, pp. 716–726. ISSN: 0141-0296. DOI: 10.1016/j.engstruct.
 326 2013.10.032. URL: <https://www.sciencedirect.com/science/article/pii/S0141029613005014> (visited on 08/21/2024).
- 327
- 328 Bendsøe, Martin P. and Ole Sigmund (2004). "Topology Optimization by
 329 Distribution of Isotropic Material". In: *Topology Optimization: Theory,
 330 Methods, and Applications*. Ed. by Martin P. Bendsøe and Ole Sigmund.
 331 Berlin, Heidelberg: Springer, pp. 1–69. ISBN: 978-3-662-05086-6. DOI: 10.
 332 1007/978-3-662-05086-6_1. URL: https://doi.org/10.1007/978-3-662-05086-6_1 (visited on 08/21/2024).
- 333
- 334 Cea, Jean (1986). "Conception Optimale Ou Identification de Formes, Calcul
 335 Rapide de La Dérivée Directionnelle de La Fonction Coût". In: *ESAIM: Modélisation mathématique et analyse numérique* 20.3, pp. 371–402. ISSN:
 336 1290-3841. URL: http://www.numdam.org/item/M2AN_1986__20_3_371_0/ (visited on 08/22/2024).
- 337
- 338
- 339 Cervelli, P. et al. (2001). "Estimating Source Parameters from Deformation
 340 Data, with an Application to the March 1997 Earthquake Swarm off the
 341 Izu Peninsula, Japan". In: *Journal of Geophysical Research: Solid Earth*
 342 106.B6, pp. 11217–11237. ISSN: 2156-2202. DOI: 10.1029/2000JB900399.
 343 URL: <https://onlinelibrary.wiley.com/doi/abs/10.1029/2000JB900399>
 344 (visited on 08/22/2024).
- 345
- 346 Charco, M. and P. Galán del Sastre (Mar. 1, 2014). "Efficient Inversion of
 347 Three-Dimensional Finite Element Models of Volcano Deformation". In:
 348 *Geophysical Journal International* 196.3, pp. 1441–1454. ISSN: 0956-540X.
 349 DOI: 10.1093/gji/ggt490. URL: <https://doi.org/10.1093/gji/ggt490> (visited on 08/22/2024).
- 350
- 351 Dapogny, Charles and Eric Bonnetier (2024). *An Introduction to Shape and*
 352 *Topology Optimization*. URL: <https://membres-ljk.imag.fr/Charles.Dapogny/coursoptim.html> (visited on 08/21/2024).
- 353

- 353 Dapogny, Charles and Florian Feppon (Oct. 31, 2023). “Shape Optimiza-
 354 tion Using a Level Set Based Mesh Evolution Method: An Overview and
 355 Tutorial”. In: *Comptes Rendus. Mathématique* 361.G8, pp. 1267–1332.
 356 ISSN: 1778-3569. DOI: 10.5802/crmath.498. URL: <https://comptes-rendus.academie-sciences.fr/mathematique/articles/10.5802/crmath.498/> (visited on 08/02/2024).
- 359 — (July 30, 2024). *Dapogny/Sotuto*. URL: <https://github.com/dapogny/sotuto> (visited on 08/21/2024).
- 361 Dzurisin, Daniel (2007). *Volcano Deformation: Geodetic Monitoring Tech-
 362 niques*. Springer-Praxis Books in Geophysical Sciences. Berlin ; New York
 363 : Chichester, UK: Springer ; Praxis. 441 pp. ISBN: 978-3-540-42642-4.
- 364 Feppon, F. et al. (Sept. 15, 2020). “Topology Optimization of Thermal Fluid–Structure
 365 Systems Using Body-Fitted Meshes and Parallel Computing”. In: *Jour-
 366 nal of Computational Physics* 417, p. 109574. ISSN: 0021-9991. DOI: 10.
 367 1016/j.jcp.2020.109574. URL: <https://www.sciencedirect.com/science/article/pii/S002199912030348X> (visited on 08/22/2024).
- 369 Frei, Walter (Dec. 29, 2015). *Designing New Structures with Shape Optimiza-
 370 tion*. COMSOL. URL: <https://www.comsol.com/blogs/designing-new-structures-with-shape-optimization> (visited on 08/22/2024).
- 372 Geuzaine, Christophe, Jean-Francois Remacle, and P Dular (2009). “Gmsh:
 373 A Three-Dimensional Finite Element Mesh Generator”. In: *International
 374 Journal for Numerical Methods in Engineering* 79.11, pp. 1309–1331.
- 375 Greiner, Sonja HM (2021). “Including Topography and a 3D-elastic Structure
 376 into a Finite-Element Deformation Model of Grímsvötn, Iceland”. PhD
 377 thesis. URL: <http://hdl.handle.net/1946/38435>.
- 378 Hadamard, J. (1908). *Mémoire Sur Le Problème d’analyse Relatif a l’équilibre
 379 Des Plaques Élastiques Encastrées*. Académie Des Sciences. Mémoires.
 380 Imprimerie nationale. URL: <https://books.google.co.ma/books?id=8wSUmAEACAAJ>.
- 382 Hecht, F. (2012). “New Development in FreeFem++”. In: *Journal of Nu-
 383 matical Mathematics* 20.3-4, pp. 251–265. ISSN: 1570-2820. URL: <https://freefem.org/>.
- 385 Hickey, James and Joachim Gottsmann (June 2014). “Benchmarking and De-
 386 veloping Numerical Finite Element Models of Volcanic Deformation”. In:
 387 *Journal of Volcanology and Geothermal Research* 280, pp. 126–130. ISSN:
 388 03770273. DOI: 10.1016/j.jvolgeores.2014.05.011. URL: <https://linkinghub.elsevier.com/retrieve/pii/S037702731400153X> (vis-
 390 ited on 02/29/2024).
- 391 Hunter, William et al. (2017). *ToPy - Topology Optimization with Python*.
 392 GitHub. URL: <https://github.com/williamhunter/topy>.

- 393 Íslands, Landmælingar (2024). *ISN2016 - Tækniskýrsla*. Landmælingar Ís-
394 lands. URL: <https://www.lmi.is/is/um-lmi/frettagfirlit/isn2016-tkniskrsla> (visited on 08/22/2024).
- 395
- 396 Le Quilliec, Guenael (2014). "Topology Optimization Procedure TOPOP-
397 TIM and Other Various Developments Made with Cast3M". In: DOI:
398 10.13140/2.1.2718.3682. URL: <http://rgdoi.net/10.13140/2.1.2718.3682> (visited on 02/29/2024).
- 399
- 400 McTigue, D. F. (Nov. 10, 1987). "Elastic Stress and Deformation near a Fi-
401 nite Spherical Magma Body: Resolution of the Point Source Paradox". In: *Journal of Geophysical Research: Solid Earth* 92.B12, pp. 12931–
402 12940. ISSN: 0148-0227. DOI: 10.1029/JB092iB12p12931. URL: <https://agupubs.onlinelibrary.wiley.com/doi/10.1029/JB092iB12p12931>
403 (visited on 02/27/2024).
- 404
- 405
- 406 Mogi, Kiyoo (1958). "Relations between the Eruptions of Various Volcanoes
407 and the Deformations of the Ground Surfaces around Them". In: *Earthq Res Inst* 36, pp. 99–134.
- 408
- 409 Parks, Michelle et al. (Jan. 23, 2024). "Data and Geodetic Modelling Results
410 for Science Article "Fracturing and Tectonic Stress Drives Ultra-Rapid
411 Magma Flow into Dikes"". In: URL: <https://osf.io/9rcq7/> (visited on
412 08/21/2024).
- 413
- 414 Sigmund, O. (Apr. 1, 2001). "A 99 Line Topology Optimization Code Writ-
415 ten in Matlab". In: *Structural and Multidisciplinary Optimization* 21.2,
416 pp. 120–127. ISSN: 1615-1488. DOI: 10.1007/s001580050176. URL: <https://doi.org/10.1007/s001580050176> (visited on 08/22/2024).
- 417
- 418 Sigmund, Ole and Kurt Maute (Dec. 1, 2013). "Topology Optimization Ap-
419 proaches". In: *Structural and Multidisciplinary Optimization* 48.6, pp. 1031–
420 1055. ISSN: 1615-1488. DOI: 10.1007/s00158-013-0978-6. URL: <https://doi.org/10.1007/s00158-013-0978-6> (visited on 08/21/2024).
- 421
- 422 Sigmundsson, Freysteinn et al. (Mar. 15, 2024). "Fracturing and Tectonic
423 Stress Drive Ultrarapid Magma Flow into Dikes". In: *Science* 383.6688,
424 pp. 1228–1235. DOI: 10.1126/science.adn2838. URL: <https://www.science.org/doi/10.1126/science.adn2838> (visited on 08/21/2024).
- 425
- 426 Slavov, Stoyan and Mariya Konsulova-Bakalova (Jan. 15, 2019). "Optimizing
427 Weight of Housing Elements of Two-stage Reducer by Using the Topology
428 Management Optimization Capabilities Integrated in SOLIDWORKS: A
429 Case Study". In: *Machines* 7.1, p. 9. ISSN: 2075-1702. DOI: 10.3390/
430 machines7010009. URL: <https://www.mdpi.com/2075-1702/7/1/9>
(visited on 08/22/2024).
- 431
- 432 Taylor, Nicola C., Jessica H. Johnson, and Richard A. Herd (Nov. 1, 2021).
433 "Making the Most of the Mogi Model: Size Matters". In: *Journal of
Volcanology and Geothermal Research* 419, p. 107380. ISSN: 0377-0273.

- 434 DOI: 10 . 1016 / j . jvolgeores . 2021 . 107380. URL: <https://www.sciencedirect.com/science/article/pii/S0377027321002092> (visited on 08/22/2024).
- 435
- 436
- 437 Trasatti, Elisa (July 1, 2022). "Volcanic and Seismic Source Modeling: An
438 Open Tool for Geodetic Data Modeling". In: *Frontiers in Earth Science*
439 10. ISSN: 2296-6463. DOI: 10 . 3389 /feart . 2022 . 917222. URL: <https://www.frontiersin.org/journals/earth-science/articles/10.3389/feart.2022.917222/full> (visited on 08/21/2024).
- 440
- 441
- 442 Velez, Maria Laura et al. (Apr. 30, 2011). "Deformation of Copahue Vol-
443 cano: Inversion of InSAR Data Using a Genetic Algorithm". In: *Journal*
444 *of Volcanology and Geothermal Research* 202.1, pp. 117–126. ISSN: 0377-
445 0273. DOI: 10 . 1016 / j . jvolgeores . 2011 . 01 . 012. URL: <https://www.sciencedirect.com/science/article/pii/S0377027311000394>
446 (visited on 08/22/2024).
- 447
- 448 Yang, Xue-Min, Paul M. Davis, and James H. Dieterich (1988). "Deforma-
449 tion from Inflation of a Dipping Finite Prolate Spheroid in an Elastic
450 Half-Space as a Model for Volcanic Stressing". In: *Journal of Geophys-
451 ical Research: Solid Earth* 93.B5, pp. 4249–4257. ISSN: 2156-2202. DOI:
452 10 . 1029 /JB093iB05p04249. URL: <https://onlinelibrary.wiley.com/doi/abs/10.1029/JB093iB05p04249> (visited on 08/22/2024).
- 453